JACS
JOURNAL OF THE AMERICAN CHEMICAL SOCIETY

COMMUNICATION

pubs.acs.org/JACS

Superfast Motion of Catalytic Microjet Engines at Physiological Temperature

Samuel Sanchez,* Adithya N. Ananth, Vladimir M. Fomin, Marlitt Viehrig, and Oliver G. Schmidt

Institute for Integrative Nanosciences, IFW Dresden, Helmholtzstrasse 20, D-01069 Dresden, Germany

Supporting Information

ABSTRACT: There is a great interest in reducing the toxicity of the fuel used to self-propel artificial nanomachines. Therefore, a method to increase the efficiency of the conversion of chemicals into mechanical energy is desired. Here, we employed temperature control to increase the efficiency of microjet engines while simultaneously reducing the amount of peroxide fuel needed. At physiological temperatures, i.e. 37 °C, only 0.25% H_2O_2 is needed to propel the microjets at 140 μm s^{-1}, which corresponds to three body lengths per second. In addition, at 5% H_2O_2, the microjets acquire superfast speeds, reaching 10 mm s^{-1}. The dynamics of motion is altered when the speed is increased; i.e., the motion deviates from linear to curvilinear trajectories. The observations are modeled empirically.

The quest for powerful nano- and micromachines with performance comparable to biological motors is a challenge of increasing interest in multidisciplinary fields.[1] In nature, most flagellated bacteria move at relative speeds of about 25−100 body lengths per second, representing one of the fastest organisms on Earth.[2] Since the pioneering works on catalytic motors,[3] considerable effort has been put toward the efficient conversion of chemicals into mechanical energy, challenging artificial machines to reach speeds comparable to those of the biological motors.

To approach that impressive speed, however, researchers used toxic chemicals such as hydrazine[4] and high concentrations of hydrogen peroxide,[5] which renders the implementation of the artificial nanomotors in real biological samples practically impossible. Small, engineered, self-propelled catalytic motors are based on the breakdown of H_2O_2 into O_2 and H_2O, as recently reviewed by several groups.[6] Tubular microjet engines based on rolled-up nanotechnology[7] present some advantages compared to other man-made nanomotors: larger surface area, on-demand tuning of materials and dimensions, mass production, and reproducibility.[6g,8] In addition, microtubular jet engines rely on the bubble propulsion mechanism, which is not affected by the ionic strength of the solution.[9] Microjets engines are capable of transporting large microobjects[10,11] and cells[12,13] in different media. However, some challenges remain, such as reducing the high toxicity of the fuel and finding the maximum speed the microjets can acquire. Reducing the concentration of peroxide fuel would permit the manipulation of living cells for long periods, whereas faster microjets would imply higher propulsion power to carry heavy loads.

Here, we demonstrate and report for the first time that both the dramatic acceleration of rolled-up microjet engines and the reduction of peroxide toxicity can be achieved by heating the fuel solution to physiological temperature (i.e., 37 °C). Moreover, the speed of the microjet engines can be tuned by modulating the temperature. We observe a change in the dynamics of tubular microjets with the temperature, and the behavior is theoretically modeled. We also present superfast catalytic self-propelled microengine/motor (~200 body lengths per second, bl s^{-1}) using only 5% H_2O_2 as fuel. In addition, we report on the lowest concentration of peroxide used for powering any catalytic nano- or micromotor (i.e., in 0.25% H_2O_2).

Microjets were fabricated by rolled-up nanotechnology on polymers as reported elsewhere[6g,8] in detail and in the Supporting Information. The rolled-up microtubes consist of Ti/Cr/Pt nanomembranes (10:5:1 nm) deposited onto photoresist patterns of 50 μm^2. The temperature was controlled by two Peltier elements set up in connection with a dc power supply (Hameg Instruments) placed underneath the sample containing the microjets suspension in H_2O_2. Cooling of the system was carried out by applying a suitable current; reversing the bias resulted in heating the Peltier element—every 0.1 A increment of applied current resulted in a 5 °C change in the temperature of 1 mL of solution. Peltier elements used in this work (15 × 15 × 4.9 mm, $l \times w \times h$) can achieve a maximum power of 3.9 W and current of 3 A, where the nominal voltage can be up to 1.9 V. The temperature was monitored using a digital thermometer immersed into the solution containing the microjets.

Since one of our goals is to study the self-propulsion of microjets in fuels and environments that are more biocompatible than those reported so far, we investigated the dependence of microjet speed on the temperature at low concentration of H_2O_2, i.e., 1% (v/v) with 0.5% surfactant to reduce the surface tension[14] (Figure 1A). Surfactant was purchased from Fit GmbH and was composed of 5−15% anionic tenside (5−15%), amphoteric tenside (<5%), Bronopol, benzisothiazolinone, and methylisothiazolinone. The temperature was adjusted to 0, 5, 10, 15, 20, 27, and 37 °C. The respective videos of the microjets, which are available in the Supporting Information (SI), were recorded at 50 frames per second. The 50 μm long microtubular engines overcome Brownian motion at about 10 °C, where they move at an average speed of 50 μm s^{-1} (1 bl s^{-1}). Between 5 and 20 °C, the speed increases in a quadratic way (Figure 1A). In contrast, when the temperature is higher than 20 °C, the temperature−speed dependence follows a linear trend, giving a final sigmoidal trend. The viscosity of the fuel solution was also measured for the studied range of temperatures (Figure 1A, blue y-axis). The dynamic viscosity diminishes from 1.7 to 0.9 mPa·s when the temperature is increased from 5 to 37 °C. Based on the linear expression of Stokes's law, this decrease in the viscosity of

Received: May 31, 2011
Published: August 17, 2011

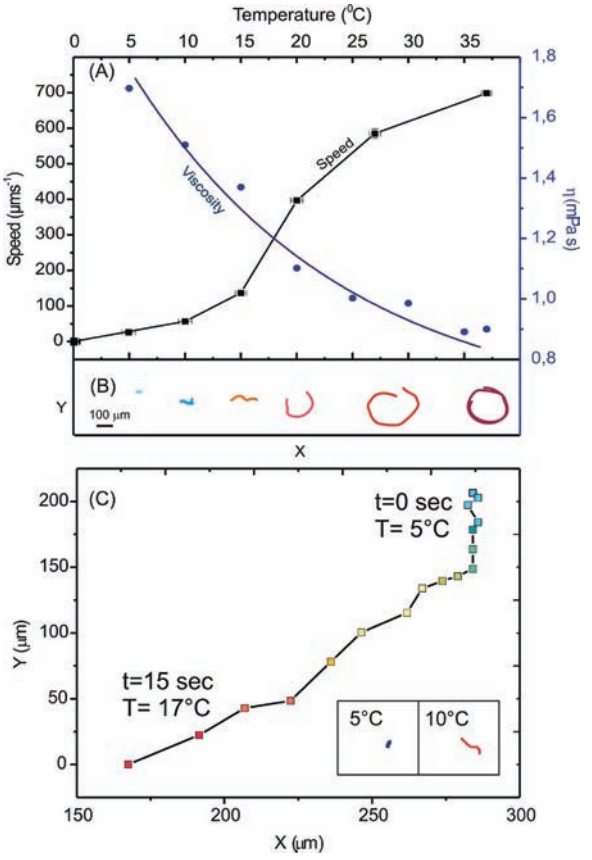

Figure 1. (A) Speed of catalytic microjet engines (left, black *y*-axis) and viscosity of the fuel (right, blue *y*-axis) versus temperature. (B) Tracking trajectories of microjet engines at temperatures from 5 to 37 °C during 1 s. Fuel solution, 1% H_2O_2 containing 0.5% surfactant. (C) Acceleration of a microengine which was previously stopped by cooling the fuel solution to 5 °C. Insets depict the tracking of the microjet at 5 and 10 °C during 1 s. (See corresponding videos in the SI for all tracking motions.)

the solution should increase the velocity of the microengines in the same manner, meaning that the speed should be nearly doubled. However, that is not the case, since the observed speed follows almost a sigmoidal behavior, which can be differentiated into two regimes: a quadratic and a linear term dependent on the temperature. Furthermore, it is well known that an increase of the temperature of the solution promotes mass transport through convection, accelerating the kinetics of the chemical reactions (here, hydrogen peroxide oxidation to oxygen). Both effects might influence the pronounced increase of speed at low temperatures. Nonetheless, a change in the dynamics of the microjets is observed from linear to circular trajectories with increasing temperature, as depicted in the tracking trajectories in Figure 1B and corresponding videos in the SI.

This behavior can be explained within an empirical model of the temperature-dependent dynamics of microjets based on the equations of motion for the translational and rotational degrees of freedom. In agreement with Purcell,[15] the motion of the microjet can be described by neglecting inertia at low Reynolds numbers (here calculated to be from $Re = 10^{-4}$ to 10^{-2}). The velocity v is then determined from the equilibrium between the driving force and the damping force, which are assumed to act respectively along and opposite to the velocity (see Figure 2),

$$F_{\mathrm{jet}} = F_{\mathrm{damp}}(v) \tag{1}$$

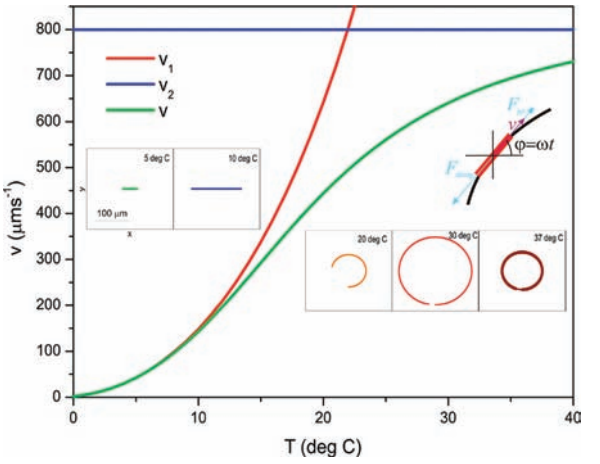

Figure 2. Calculated speed of catalytic microjet engines for linear (red), quadratic (blue), and combined superlinear (green) drag models. The scheme represents the driving (jet) and damping forces with assumed denotations. The velocity is assumed along the main axis of a cylindrical microjet. Insets depict the trajectories of the microjet at selected temperatures during 1 s (the same colors as in Figure 1B).

while the angular frequency $\omega = \mathrm{d}\varphi/\mathrm{d}t$ is determined from the equilibrium between the driving torque and the damping torque,

$$\tau_{\mathrm{jet}} = \tau_{\mathrm{damp}}(\omega) \tag{2}$$

For the damping force, we assume a combination of the common linear and quadratic terms,

$$F_{\mathrm{damp}}(v) = c(T)v + bv^2 \tag{3}$$

The coefficient in the linear Stokes-like damping force is $c(T) = 6\pi\eta(T)l$, where l is the effective microjet size. The viscosity $\eta(T)$ in the model is a decaying function of temperature, taken as a linear extrapolation through the experimental data in Figure 1, $\eta(5\,^{\circ}\mathrm{C}) = 1.70$ mPa·s and $\eta(40\,^{\circ}\mathrm{C}) = 0.90$ mPa·s. The driving force F_{jet}, due to the jet effect, is supposed to be independent of velocity: $F_{\mathrm{jet}} = c(5\,^{\circ}\mathrm{C})(30\ \mu\mathrm{m\cdot s^{-1}})[(1 + 3T/4)^2/16]$.

A purely linear damping force (when $b = 0$ in eq 3) according to eq 1 leads to the velocity $v_1 = F_{\mathrm{jet}}/c(T)$, which is a monotonically rising function of temperature (Figure 2). This is in contradiction to the experimental observation (Figure 1). Quadratic drag forces are widely invoked for the interpretation of dynamics of realistic systems at various scales, ranging from the motion of marine vehicles[16] through micro- and nanoelectromechanical systems with symmetry breaking,[17,18] to flapping flyers[19] and microjets.[20] In different systems, various physical mechanisms underlie the occurrence of the quadratic drag forces, e.g., the existence of a boundary layer in the fluid near the moving microjet.[21] The excitation of slow drift eddy currents (vortices) is shown to produce important quadratic damping force for sway and yaw motion of a moving object, while those eddy currents are much less important for its surge motion[22] (see eq 8 in ref 22).

In particular, for the case of microjet engines, at low speeds ($v < 200\ \mu\mathrm{m\ s^{-1}}$) there is a negligible contribution of the eddy flows. Consequently, the trajectory remains straight, and the experienced force is linear. However, at high speeds ($v > 200\ \mu\mathrm{m\ s^{-1}}$) the motion deviates from the linear trajectory, thus promoting the excitation of eddy flows. Because of that, the drag force acquires a certain quadratic contribution. Additional support for our assumption is provided by the clear correlation between the speed of a

microjet engine due to the quadratic drag force (Figure 2) and the development of the curvilinear trajectories of the microjet engine (insets to Figure 2). Therefore, we imply in eq 3 a quadratic damping force acting on the catalytic microjet engine. In a model with a purely quadratic damping force ($c(T) = 0$), the velocity, found according to eq 1, is $v_2 = (F_{jet}/b)^{1/2}$. For the purpose of the calculation, the coefficient $b = F_{jet}/(800\ \mu m\ s^{-1})^2$ is selected, providing the velocity v_2 independent of temperature (Figure 2).

The microjet velocity,

$$v = \sqrt{(v_2^2/2v_1)^2 + v_2^2} - v_2^2/2v_1 \quad (4)$$

resulting from eq 1 with a full damping force (eq 3) is represented in Figure 2 as a function of temperature. The behavior of v reveals a transition from a superlinear increase at low temperatures near 5 °C through an almost linear regime at ~20 °C to a sublinear increase at higher temperatures, in excellent agreement with the experimental data shown in Figure 1. With temperatures higher than 40 °C, the microjet velocity tends to saturate at the value of v_2. The transition at T ~20 °C can thus be attributed to the change of the damping force regime from predominantly linear at lower temperatures to superlinear at higher temperatures. The transition is smooth: in the region T ~20 °C the quadratic component in the damping force constitutes about one-third of the linear component, while at T ~30 °C the quadratic component becomes larger than the linear one.

The observed trajectories are linear at lower temperatures and curvilinear at higher temperatures. This fact suggests assigning to the torque, which drives the rotation of a microjet around its axis perpendicular to the main axis, nonzero values at elevated temperatures larger than 18 °C. It emerges presumably by virtue of the jet effect from the bubbles, which leave the microjet at a certain angle with respect to its main axis. We select the values τ_{jet} independent of angular frequency to fit the shape of the observed microjet tracks (Figure 1). The damping torque is taken to be linear with respect to the angular frequency,

$$\tau_{damp}(\omega) = \gamma\omega \quad (5)$$

where the drag coefficient $\gamma = \kappa V\eta$ is determined by volume V of the microjet, the viscosity η, and a microjet shape factor κ.[23] The angular frequency is then $\omega = \tau_{jet}/\gamma$. Finally, microjet trajectories, which result from integrating the obtained velocities with the components,

$$v_x(t) = v\cos\omega t, \quad v_y(t) = v\sin\omega t \quad (6)$$

(insets in Figure 2), compare well with experiment (Figure 1B).

The ability to tune the power of self-propelled microjets has recently raised increasing interest.[4−6] By cooling the fuel solution (see corresponding videos in the SI), the microjets can be completely brought to a halt at temperatures of about 2 °C. Figure 1C depicts the positions and swimming distances of a microjet engine which starts to self-propel upon increasing the temperature from 5 to 17 °C. Each point in the plot represents the position of the microjet every second, and the insets show the tracking motion of a microjet at 5 and 10 °C (Figure 1A,B) during a period of 1 s. It is clear that the distance between two consecutive points becomes larger with increasing temperature, indicating a continuous acceleration of the jets.

The enhancement of the catalytic turnover rate by heating the solution allows us to use very low concentrations of peroxide fuel, hence reducing its toxicity. Figure 3 shows optical images and the tracking trajectories of microjets in 0.25, 0.5, 1, and 2% H_2O_2,

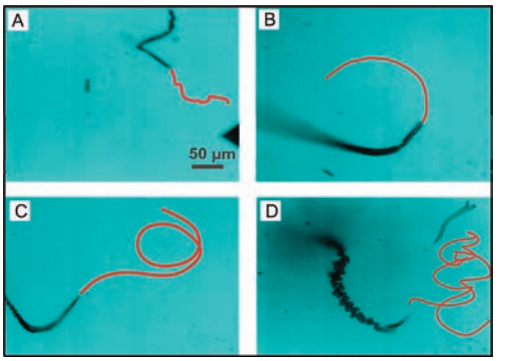

Figure 3. Optical images including tracking trajectories of catalytic microjet engines at different hydrogen peroxide concentrations: (A) 0.25, (B) 0.5, (C) 1, and (D) 2% H_2O_2. Temperature of the solution was kept constant at 37 °C. (See corresponding videos in the SI.)

swimming along 140, 235, 700, and 2000 μm, respectively, during 1 s at 37 °C. Previously, we reported the extraordinary decrease of toxicity by modifying the inside of the microtubes with catalase enzyme, propelling at 10 bl s^{-1} (250 $\mu m\ s^{-1}$) in 1.5% H_2O_2.[24] As a comparison, the microjets move at speeds similar to those of the catalase-based hybrid microjets by using 3 times lower concentration of peroxide fuel when the temperature is set to 37 °C. These results are promising for the development of man-made machines which self-propel in environments of reduced toxicity and at temperatures where cells grow.

To test the toxicity of the fuel, we performed MTT ((3-(4,5-dimethylthiazol-2-yl)-2,5-diphenyltetrazolium bromide) viability assay (Sigma, Germany) for fibroblast NIH-3T3 cell lines. The NIH-3T3 fibroblasts were grown in Dulbecco's Modified Eagle Medium, 10% fetal calf serum, and 1% penicillin/streptomycin antibiotics. The cells were incubated during 24 h in a humidified atmosphere in 5% CO_2 at 37 °C until they had grown to ~3 × 10^5 cells/mL. The cell culture was then treated with different concentrations of H_2O_2, 0, 0.1, 0.25, 0.5, 1, and 2% (v/v), for 30 and 60 min. After the appropriate treatment time, the culture medium containing H_2O_2 was discarded, and the cells were rinsed with 1× phosphate-buffered saline three times to wash away H_2O_2 residues. Afterward, fresh culture medium and MTT (10:1) solution (5 mg/mL MTT in RPMI-1640 without phenol red) were added to the cell culture and incubated for 4 h at 37 °C and 5% CO_2. The medium was discarded and the same volume of MTT solvent (0.1 N HCl in anhydrous isopropanol) added to dissolve formazan created by the MTT. The absorbance was measured spectrophotometrically within 1 h after the addition of the MTT solvent at 570 nm and with reference wavelength at 690 nm. Each experiment was carried out in triplicate.

The results show that after 1 h of treatment with 0.25% H_2O_2, about 40% of the cells are viable, whereas at 1 and 2% H_2O_2 only 20 and 15% of the cells are viable, respectively. If the cells are treated for 30 min with 1% H_2O_2, the viability is 3 times higher, reaching 60%. Nonetheless, our results foresee the necessity of reducing the amount of peroxide in the fuel solution (lower than 1% H_2O_2) to extend the time the microjets could interact with viable cells. Thus, by controlling the temperature of the solution, we also can keep more cell-friendly environments (less toxic and physiological temperature) than those previously reported where self-propelled microjets move at considerably high speeds.

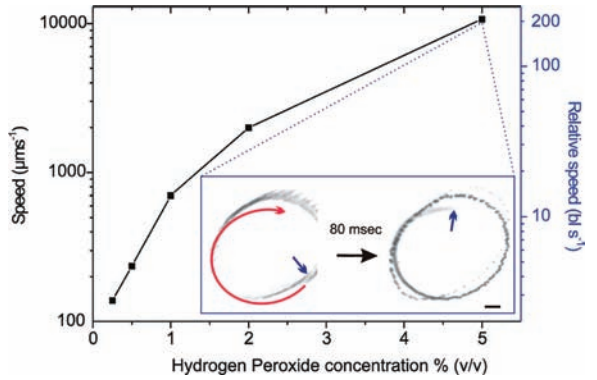

Figure 4. Absolute (left *y*-axis) and relative (right *y*-axis) speeds of catalytic microjet engines at 37 °C with increasing concentrations of hydrogen peroxide. Inset figure tracks (red line) the trajectory of an ultrafast microjet at 5% H_2O_2 at 37 °C. The blue arrow points at the front edge of the microtube. (Two videos of the superfast motion are available in the SI.)

Can the catalytic microjets compete with the speed of biomotors? Figure 4 shows the absolute and relative speeds of the microjets at 37 °C with different concentrations of H_2O_2 from 0.25 to 5% (v/v). Under these conditions, the microjets can reach absolute speeds of about 10 mm s^{-1}, corresponding to a relative speed of 200 bl s^{-1}. Thus, we are reporting superfast catalytic self-propelled engines, with speed comparable to that of some bacteria (50−150 bl s^{-1}). The inset in Figure 4 depicts an optical sequence of the fastest microjet with a time lapse of 80 ms, recorded by a high-speed camera. The blue arrow points at the microjet position, and the red line tracks the trajectory during that time. The curvilinear motion at very high speeds is in concordance with the previous obserations at fast speeds (Figure 1) and the empirical model described in this work (Figure 2).

In conclusion, we have demonstrated the ability of microjet engines to propel at very low concentrations of peroxide fuel by heating the solution to physiological temperature. Such conditions should allow for future investigations combining catalytic microjets with living cells over long periods for different applications. The ultrafast speed achieved by the microjets is of importance for the design of highly powered micro- and nanomachines, thus enabling transport of heavy loads or swimming over long distances. The dynamics of the catalytic microjets have been theoretically modeled and fit well with the experimental observations. This theoretical work can pave the way to future physical investigations of the single and collective motion of self-propelled micromachines.

■ ASSOCIATED CONTENT

Supporting Information. Videos for all the presented data (.avi) and details of the preparation of rolled-up microtubes. This material is available free of charge via the Internet at http://pubs.acs.org.

■ AUTHOR INFORMATION

Corresponding Author
s.sanchez@ifw-dresden.de

■ ACKNOWLEDGMENT

The authors thank C. Krien and R. Engelhard for help with preparation of samples and J. Scheiter for the viscosity measurements. We thank A. A. Solovev and the NanoBioChem group for discussions. This work was funded by the Volkswagen Foundation (I/84 072).

■ REFERENCES

(1) (a) Ozin, G. A.; Manners, I.; Fournier, S. B.; Arsenault, A. *Adv. Mater.* **2005**, *17*, 3011–3018. (b) van den Heuvel, M. G. L.; Dekker, C. *Science* **2007**, *317*, 333–336. (c) Sen, A.; Ibele, M.; Hong, Y.; Velegol, D. *Faraday Discuss.* **2009**, *143*, 15–27.

(2) Stocker, R.; Seymour, J. R.; Samadani, A.; Hunt, D. E.; Polz, M. F. *Proc. Natl. Acad. Sci. U.S.A.* **2008**, *105*, 4209–4214.

(3) Ismagilov, R. F.; Schwartz, A.; Bowden, N.; Whitesides, G. M. *Angew. Chem., Int. Ed.* **2002**, *41*, 652. (b) Paxton, W. F.; Kistler, K. C.; Olmeda, C. C.; Sen, A.; St. Angelo, S. K.; Cao, Y.; Mallouk, T. E.; Lammert, P. E.; Crespi, V. H. *J. Am. Chem. Soc.* **2004**, *126*, 13424. (c) Fournier-Bidoz, S.; Arsenault, A. C.; Manners, I.; Ozin, G. A. *Chem. Commun.* **2005**, 441.

(4) Laocharoensuk, R.; Burdick, J.; Wang, J. *ACS Nano* **2008**, *2*, 1069–1075.

(5) Demirok, U. K.; Laocharoensuk, R.; Manesh, K. M.; Wang, J. *Angew. Chem., Int. Ed.* **2008**, *47*, 9349–9351.

(6) (a) Paxton, W. F.; Sundararajan, S.; Mallouk, T. E.; Sen, A. *Angew. Chem., Int. Ed.* **2006**, *45*, 5420–5429. (b) Mallouk, T. E.; Sen, A. *Sci. Am.* **2009**, *300*, 72–77. (c) Wang, J. *ACS Nano* **2009**, *3*, 4–9. (d) Sanchez, S.; Pumera, M. *Chem.—Asian J.* **2009**, *4*, 1402–1410. (e) Pumera, M. *Nanoscale* **2010**, *2*, 1643–1649. (f) Mirkovic, T.; Zacharia, N. S.; Scholes, G. D.; Ozin, G. A. *ACS Nano* **2010**, *4*, 1782–1789. (g) Mei, Y. F.; Solovev, A. A.; Sanchez, S.; Schmidt, O. G. *Chem. Soc. Rev.* **2011**, *40*, 2109–2119.

(7) Schmidt, O. G.; Eberl, K. *Nature* **2001**, *410*, 168.

(8) Mei, Y. F.; Huang, G. S.; Solovev, A. A.; Bermúdez-Ureña, E.; Mönch, I.; Ding, F.; Reindl, T.; Fu, R. K. Y.; Chu, P. K; Schmidt, O. G. *Adv. Mater.* **2008**, *20*, 4085–4090.

(9) Manesh, K. M.; Cardona, M.; Yuan, R.; Clark, M.; Kagan, D.; Balasubramanian, S.; Wang, J. *ACS Nano* **2010**, *4*, 1799–1804.

(10) Solovev, A. A.; Sanchez, S.; Pumera, M.; Mei, Y. F.; Schmidt, O. G. *Adv. Funct. Mater.* **2010**, *20*, 2430–2435.

(11) Sanchez, S.; Solovev, A. A.; Harazim, S. M.; Schmidt, O. G. *J. Am. Chem. Soc.* **2011**, *133*, 701–703.

(12) Sanchez, S.; Solovev, A. A.; Schulze, S.; Schmidt, O. G. *Chem. Commun.* **2011**, *47*, 698–700.

(13) Balasubramanian, S.; Kagan, D.; Hu, C.-M. J.; Campuzano, S.; Lobo-Castanon, M. J.; Lim, N.; Kang, D. Y.; Zimmerman, M.; Zhang, L.; Wang, J. *Angew. Chem., Int. Ed.* **2011**, *50*, 4161–4164.

(14) Solovev, A. A.; Mei, Y. F.; Schmidt, O. G. *Small* **2009**, *5*, 1688–1692.

(15) Purcell, E. M. *Am. J. Phys.* **1977**, *45*, 3–11.

(16) Fossen, T. I. *Guidance and Control of Ocean Vehicles*; John Wiley & Sons: New York, 1994.

(17) Lifshitz, R.; Cross, M. C. In *Reviews of Nonlinear Dynamics and Complexity*; Schuster, H. G., Ed.; Wiley-VCH: Berlin, 2008; Vol. 1, section 1.2.3 (available at www.tau.ac.il/~ronlif/pubs/RNDC1-1-2008-preprint.pdf).

(18) Eichler, A.; Moser, J.; Chaste, J.; Zdrojek, M.; Wilson-Rae, I.; Bachtold, A. *Nature Nanotechnol.* **2011**, *6*, 339–342.

(19) Ramananarivo, S.; Godoy-Diana, R.; Thiria, B. arXiv:1011.4688v1 [physics.bio-ph], 2010 (http://arxiv.org/abs/1011.4688).

(20) Pawashe, C.; Floyd, S.; Sitti, M. *Int. J. Robot. Res.* **2009**, *28*, 1077–1094.

(21) Munson, B.; Young, D.; Okiishi, T. *Fundamentals of Fluid Mechanics*, 4th ed.; JohnWiley and Sons, Inc.: New York, 2002.

(22) Faltinsen, O. M.; Sortland, B. *Appl. Ocean Res.* **1987**, *9*, 37–46.

(23) Tirado, M. M.; Martínez, C. L.; de la Torre, J. G. *J. Chem. Phys.* **1984**, *81*, 2047.

(24) Sanchez, S.; Solovev, A. A.; Mei, Y. F.; Schmidt, O. G. *J. Am. Chem. Soc.* **2010**, *132*, 13144–13145.

■ NOTE ADDED AFTER ASAP PUBLICATION

This article was published ASAP on August 23, 2011. Reference 1a was incorrectly listed. The corrected version was posted on August 31, 2011.